Protein and metal cluster structure of the wheat metallothionein domain γ-E_c-1. The second part of the puzzle.

Jens Loebus[§] · Estevão A. Peroza[§] · Nancy Blüthgen · Thomas Fox · Wolfram Meyer-Klaucke · Oliver Zerbe · Eva Freisinger

Jens Loebus · Estevão A. Peroza · Nancy Blüthgen · Thomas Fox · Eva Freisinger (✉)
Institute of Inorganic Chemistry, University of Zurich,
8057 Zurich, Switzerland
e-mail: freisinger@aci.uzh.ch

Wolfram Meyer-Klaucke
European Molecular Biology Laboratory (EMBL), Outstation Hamburg at Deutsches Elektronen-Synchrotron (DESY),
22603 Hamburg, Germany

Oliver Zerbe (✉)
Institute of Organic Chemistry, University of Zurich,
8057 Zurich, Switzerland
e-mail: zerbe@oci.uzh.ch

[§] both authors contributed equally

Abstract Metallothioneins (MTs) are small cysteine-rich proteins, coordinating various transition metal ions including Zn^{II}, Cd^{II}, and Cu^{I}. MTs are ubiquitously present in all phyla indicating a successful molecular concept for metal ion binding in all organisms. The plant MT E_c-1 from *Triticum aestivum*, common bread wheat, is a Zn^{II} binding protein that comprises two domains and binds up to six metal ions. The structure of the C-terminal four metal ion binding β_E-domain was recently described. Here we present now also the structure of the N-terminal second domain, γ-E_c-1, determined with NMR spectroscopy. The γ-E_c-1 domain enfolds a $M^{II}_2Cys_6$ cluster and was characterized as part of the full-length Zn_6E_c-1 protein as well as in form of the separately expressed domain, both in the Zn^{II}- and the Cd^{II}-containing isoform. EXAFS analysis of $Zn_2\gamma$-E_c-1 clearly shows the presence of a ZnS_4 coordination sphere with average Zn-S distances of 2.33 Å. ^{113}Cd NMR experiments were used to identify the M^{II}-Cys connectivity pattern, revealing two putative metal cluster conformations. In addition, the general metal ion coordination abilities of γ-E_c-1 were probed with Cd^{II} binding experiments as well as by pH titrations of the Zn^{II}- and Cd^{II}-forms, the latter suggesting an interaction of the γ- and the β_E-domain within the full-length protein.

Keywords Plant metallothionein · Metal-thiolate cluster · Electronic absorption spectroscopy · EXAFS · NMR spectroscopy

Introduction

Metallothioneins (MTs) are low molecular mass (2–10 kDa) and cysteine-rich proteins with a preference for the coordination of metal ions with d^{10} electron configuration, e.g. Zn^{II}, Cu^{I}, and Cd^{II} [1]. Their occurrence is reported throughout the animal kingdom, in plants, several eukaryotic microorganisms, as well as in some prokaryotes [2]. The plant MT E_c-1 from wheat consists of 81 amino acids. All of the 17 cysteine and two histidine residues are involved in the coordination of six divalent metal ions that are arranged in two separate metal-binding domains (Figure 1) [3].

>> insert Figure 1 here (double column) <<

E_c-1 is the first and so far only plant MT, which could be successfully isolated from plant material [4]. E_c-1 is most abundant in wheat embryos and present in the Zn^{II} form [5]. Unlike the majority of MTs, E_c-1 recruits also two His residues for Zn^{II} binding, a feature so far only observed in a cyanobacterial MT form [6]. This ligand specificity usually distinguishes MTs from Zn^{II} binding enzymes, where the Zn^{II} coordination sphere often consists of a mixture of S, N, and O donor ligands. In consequence, the resulting metal clusters show a limited variety of possible structures. This is demonstrated by the fact that only two basic cluster arrangements have been structurally described for divalent metal ions so far: The $M^{II}_3Cys_9$ cluster of the β-domain of vertebrate, crustacean, and echinodermata MTs and the $M^{II}_4Cys_{11}$ cluster of the α-domain from vertebrates and echinodermata MTs (e.g. PDB codes 4MT2, 1DMC, 1DME, 1QJK, and 1QJL [7-9]). The $Zn_4Cys_9His_2$ cluster of the cyanobacterium *Synechococcus* PCC 7942 is structurally related to the Zn_4Cys_{11} cluster with exchange of two terminal thiolate ligands by imidazole moieties [6]. A Zn_3Cys_9 cluster with similarity to the $M^{II}_3Cys_9$ cluster mentioned above can be also found in the β_E-domain of wheat E_c-1, but the Zn^{II} coordinating residues are interleaved with the two Cys and His ligands of the additional mononuclear Zn^{II} site [10]. This $ZnCys_2His_2$ site, while known from certain Zn-finger

proteins, was unprecedented in the MT superfamily and is so far uniquely found in the plant E_c proteins. The limited structural variability of the metal ion binding sites in MTs goes along with the constricted biological functionality known so far, mainly the participation in metal ion homeostasis and detoxification as well as protection against oxidative stress [11-13]. Wheat E_c-1 seems to have a potential role in plant development as inferred from its high abundance during embryogenesis [8]. Interestingly, the only regulatory element found so far in the upstream 5' flanking region of the wheat E_c-1 mRNA is an abscisic acid (ABA) responsive element (ARBE) simile [14]. Even more striking than the putative regulation by one of the major plant hormones, involved in abscission, grain filling, desiccation, and embryogenesis [15], is the absence of a metal responsive regulatory element (MRE) [14]. In addition, it is known that 25% of an entire ^{35}S-labelled cysteine pool is found in E_c-1, when wheat grain embryo mRNA is expressed in a cell free expression system [4]. This indicates either a high rate of mRNA translation or a massive accumulation of E_c-1 mRNA and/or a failure of its degradation in the dried embryo, possibly regulated at the transcriptional level. From further studies, using 8K cDNA microarray technology, the E_c-1 transcript abundance was shown to correlate with grain dry weight only [16]. This behaviour is found for only three other proteins, the defence proteins γ-purothionin and remorin-like protein as well as asparagine synthetase 2, a "housekeeping" enzyme. In this study it was further shown that gene expression during wheat grain development can be divided into 10 clusters. The E_c-1 transcript belongs to the 10th cluster, which comprises only 10 of the 2295 differentially expressed genes. The E_c-1 transcript level peaks at 35 days post anthesis, hence in the maturation and desiccation state, and disappears abruptly during the first hour of imbibition [14, 16]. Generally, such rapid decline of transcripts is indicative for redundant mRNA remaining from post anthesis. This view is supported by the concomitant decrease of the E_c-1 protein level. Yet, despite the wealth of information the role of E_c-1 still remains illusive.

In the following, we will present the first three-dimensional structure of the N-terminal, 24 amino acid residues comprising, γ-domain of wheat E_c-1 as determined by NMR spectroscopy. In total, three structures of different γ-E_c-1 forms are presented: the Cd^{II} and Zn^{II} forms of the separately expressed domain as well as the Zn_2γ-E_c-1 form as part of the full-length protein. All forms contain a $M^{II}{}_2Cys_6$ cluster, which is unprecedented for any MT. EXAFS studies confirm such an arrangement. Moreover, the metal ion binding properties of γ-E_c-1 are probed via pH titration and metal ion reconstitution experiments.

Material and methods

Chemicals and solutions

$^{113}CdCl_2$ and $^{15}NH_4Cl$ were purchased from Cambridge Isotope Laboratories Inc. (Innerberg, Switzerland), d_{11}-Tris from Euriso-top (Saint-Aubin, France), enzymes used for plasmid construction and protein cleavage from Promega (Catalys AG, Wallisellen, Switzerland), Roche (Rotkreuz, Switzerland), GE Healthcare Europe GmbH (Glattbruck, Switzerland) or New England Biolabs Inc. (Ipswich, MA, USA), LB Broth (Miller) from Chemie Brunschwig AG (Basel, Switzerland) and Chelex® 100 resin from Bio-Rad (Reinach, Switzerland). All other chemicals were ACS grade or comparable and purchased from Sigma-Aldrich Chemie GmbH (Buchs, Switzerland), Calbiochem (VWR International AG, Lucerne, Switzerland) or Acros organics (Chemie Brunschwig AG, Basel, Switzerland). All solutions were prepared using degassed millipore water. If appropriate, solutions were saturated with nitrogen or argon. Whenever complete absence of oxygen was required, millipore water was degassed by three consecutive freezing thawing cycles under vacuum.

Synthetic peptide

A synthetic γ-E_c-1 peptide (purity > 90%) consisting of the first 25 amino acids of the full-length E_c-1 protein

MGCDD KCGCA VPCPG GTGCR CTSAR

was purchased from Sigma-Genosys (Haverhill, UK) and used for EXAFS, ESI-MS, pH and metal ion titration experiments as well as for the 2D ^{1}H-^{1}H TOCSY AND NOESY NMR spectra of the Cd_2γ-E_c-1 form. All other experiments were conducted with the peptide overexpressed using the pGEX-4T-gEc1 construct.

Plasmid construction

The cDNA sequence encoding for the first 24 amino acids of wheat E_c-1 without the N-terminal translation initiator Met was optimised for *E. coli* codon usage. Two additional Gly and Ser residues were added to the N-terminus of the protein to ensure optimal thrombin cleavage yielding the sequence

GS GCDD KCGCA VPCPG GTGCR CTSAR.

The resulting construct was cloned into to the pGEX-4T expression vector (GE Healthcare) using the BamH1 and EcoR1 restriction sites and the construct identity (pGEX-T4-gEc1) was subsequently verified by DNA sequencing. The constructed plasmid was transferred into the protease deficient *E. coli* expression strain BL21(DE3).

Protein expression and purification

γ-E_c-1 was overexpressed in form of the glutathione-S-transferase-MT fusion protein according to the GST purification manual (GE Healthcare). After induction with 1 mM isopropyl-β-D-thiogalactopyranosid (IPTG) at OD_{600} = 1 cells were harvested after 4 to 7 h at

37 °C and lysed by sonification. The supernatant was loaded on a pre-equilibrated GST-affinity column (GE Healthcare). After washing, the fusion protein was stripped from the column using 10 mM glutathione (GSH) and cleaved with 1 unit thrombin per mg GST-MT fusion protein for 60 h at 25 °C. Final purification of γ-E_c-1 was performed by size exclusion chromatography using a Superdex 30pg column (GE Healthcare) and the molecular identity verified with ESI-MS (Figure 2). Crucial for GST-MT protein cleavage with thrombin was the demetalation of the fusion protein with 10 mM EDTA during the GST-affinity column wash step. All chromatographic steps were conducted in 100 mM phosphate buffer saline (PBS) at pH 7.3. Purified and completely oxidized γ-E_c-1 was dialysed twice against 20 mM Tris/HCl pH 8.0, lyophilized and stored at -80 °C. Average yields are 4 mg of purified protein per L cell culture medium. The full-length E_c-1 protein was prepared as described elsewhere [3].

Apoγ-E_c-1 preparation

Apoγ-E_c-1 was prepared freshly prior to each experiment. Typically 1 to 3 mg of oxidized γ-E_c-1 was incubated with 200 mM DTT in a 100 mM Tris/HCl solution (pH 8.0) for 1 h prior to acidification to pH 2 with 1 M HCl. The sample was applied to a G10 size exclusion column (GE Healthcare) pre-equilibrated with 10 mM HCl and eluted under constant argon flow. The residual Zn^{II}, Cd^{II}, and $Cu^{I/II}$ content of apoγ-E_c-1 was below the detection limit of flame atomic absorption spectroscopy (F-AAS) (0.001 ppm). Prior to the subsequent metal ion reconstitution step, the solution of apoγ-E_c-1 was argon saturated for 1 h in a N_2-flushed glove box and the protein concentration determined via thiol quantification using the 2,2'-dithio-dipyridine (2-PDS) assay [17].

Preparation of $Zn_2\gamma$-E_c-1, Zn_6E_c-1, and $Cd_2\gamma$-E_c-1

For all experiments the exact amount of 2 or 6 equivalents of metal ions was titrated to the respective apo-form in a N_2-flushed glove box. Subsequently, the pH was raised to 8.6 using Tris-HCl or d_{11}-Tris-HCl for the NMR samples. Reconstituted samples were dialysed against 20 mM of the respective Tris-HCl solution or 5 mM NH_4Ac for ESI-MS measurements and concentrated by lyophilization.

pH Titrations followed by UV spectroscopy

800 µL of the respective reconstituted E_c-1 form (ca. 10 µM each) in 1 mM Tris-HCl 8.6 and 10 mM NaCl were titrated with diluted HCl as described [3]. For the concurrent titration of both domains, γ- and β_E-E_c-1 were mixed in equimolar amounts. Plots of molar absorptivity at 230 nm for the Zn^{II}-forms and at 250 nm for the Cd^{II}-loaded species against pH were fitted in the program Origin 7.0® (OriginLab corporation, MA, USA) using three different functions, considering either one or two common apparent pK_a values for the cysteine residues in presence of the respective metal ions as described [3, 18].

Titration of apoγ-E_c-1 with Cd^{II}

For each titration point 90 µL of 32 µM apoγ-E_c-1 were mixed with the appropriate amount of a 1.25 mM $CdCl_2$ solution in a nitrogen-purged glove box. The pH was raised to approximately 8.6 with 100 mM Tris that was pretreated with Chelex 100 resulting in samples with 20 µM E_c-1, 20 mM Tris-HCl, and 10 mM NaCl. Samples were transferred into cuvettes, sealed, and UV spectra were recorded.

Mass spectrometry

Samples of $Zn_2\gamma$-E_c-1 in 100 mM NH_4Ac (pH 8) were treated with 2 equiv. Zn^{II} or 4 equiv. Cd^{II} and injected directly or with a prior acidification step into a quadropole time-of-flight (TOF) Ultima API spectrometer (Waters, UK). 10 mM NH_4Ac in 50% MeOH (pH 7.5) or 50% acetonitrile with 0.2% formic acid (pH 2-3) were used as a solvent. Scans were accumulated and further processed by the software MassLynx 3.5 (Micromass). Deconvolution of mass spectra was done by applying the maximum entropy algorithm of the MassLynx tool MaxEnt1. Electrospray parameters were capillary 2.8 V, cone 60 V and source temperature 80 °C.

X-ray absorption spectroscopy

In order to determine the average Zn^{II} binding motif K-edge X-ray absorption spectra of $Zn_2\gamma$-E_c-1 were recorded at beamline D2 of the EMBL Outstation Hamburg at DESY, Germany, as described [19]. Data reduction, such as background removal, normalization and extraction of the fine structure, was performed with KEMP [20] assuming a threshold energy of $E_{0,Zn}$=9662 eV. The extracted K-edge EXAFS data were converted to photoelectron wave vector k-space and weighted by k^3. Initial evaluation of the spectra by ABRA [21], which is based on EXCURV [22], included a systematic screening of ~400 potential binding motifs. The subsequent meta-analysis identified structural Zn sites, and thus in the final refinement the total number of ligands was fixed to four. The absence of multiple scattering contributions indicative for the binding of imidazole rings to the Zn^{II} ion limited the refinement to the following parameters for each structural model: namely the atomic distances (R), the Debye-Waller factors ($2\sigma^2$), and a residual shift of the energy origin (EF) were refined, minimizing

the Fit Index (Φ). An amplitude reduction factor (AFAC) of 1.0 was used throughout the data analysis.

NMR spectroscopy

Zn_2^{15}N-γ-E_c-1, Cd_2^{15}N-γ-E_c-1, $^{113}Cd_2$γ-E_c-1 and Zn_6^{15}N-E_c-1 samples were prepared as described above. The lyophilised proteins were dissolved in 10% D_2O/90% H_2O, 15 mM d_{11}-Tris/HCl pH 6.9 and 50 mM NaCl to a final concentration of 1 mM protein for ^{1}H-NMR and 3 mM for ^{113}Cd-NMR studies. Proton NMR experiments to elucidate the protein backbone structure were recorded at 25 °C on Bruker Avance 700- and 600-MHz spectrometers. ^{113}Cd-NMR experiments to investigate the binding sites of the Cd^{II} ions were performed on a Bruker DRX 500-MHz spectrometer. Assignment of resonances in Cd_2γ-E_c-1 and Zn_6E_c-1 was performed using 3D ^{15}N resolved TOCSY [23, 24] and NOESY [25, 26] spectra recorded with 80 ms and 120 ms mixing times, respectively. Distance restraints were derived from the 120 ms mixing time 3D ^{15}N resolved NOESY and 2D NOESY experiments. Resonance assignments for the Zn_2γ-E_c-1 domain were conducted using 2D TOCSY and 2D NOESY spectra with 80 and 120 ms mixing times, respectively. Additionally, a 120 ms mixing time 3D ^{15}N resolved NOESY spectra as well as the information from the Cd_2γ-E_c-1 and Zn_6E_c-1 form were used to validate the assignment. Distance restraints were again derived from the 3D ^{15}N resolved NOESY and 2D NOESY experiments. In all cases zero-quantum interference in the spectra was suppressed using an appropriate filter [27, 28]. ^{15}N,^{1}H correlation maps were derived from a gradient-enhanced [^{15}N,^{1}H]-HSQC experiment using the Rance-Palmer trick for sensitivity enhancement [29, 30]. 1D-^{113}Cd-NMR**,** 2D-[^{113}Cd,^{1}H]-HSQC spectra and 2D-[^{113}Cd,^{113}Cd]-COSY experiments were recorded to investigate the metal cluster [31]. ^{3}J[H_β,Cd] couplings derived from a 2D [^{113}Cd,^{1}H]-HSQC spectrum allowed to establish the individual Cd-Cys connectivities.

Sequence-specific resonance assignment was performed using the methodology developed by Wüthrich [32]. Assignments were achieved based on information from 2D TOCSY, NOESY, 2D [^{15}N,^{1}H]-HSQC, 3D ^{15}N-resolved NOESY, and 3D ^{15}N-resolved TOCSY experiments. The 2D and 3D spectra were evaluated with the programs XEASY [33] and CARA [34], respectively. As a first step, the spin systems were identified in the 2D TOCSY or 3D ^{15}N-resolved TOCSY experiments. Subsequently, spin systems were linked based on NOE information derived from 2D NOESY and 3D ^{15}N- resolved NOESY. Once longer stretches had been identified, they were mapped onto the sequence of γ-E_c-1.

For the structure calculations NOE peaks were picked and integrated using the program XEASY for 2D and CARA for 3D experiments employing identical lower integration thresholds. Torsion angle dynamics [35] were performed with the *noeassign* [36] algorithm of the program CYANA 2.1 [37]. Structure calculations were started from 100 conformers with randomized torsion angle values. The 20 conformers with the lowest final target function value were further subjected to restrained energy minimization in explicit solvent against the AMBER force field [38] using the program OPALp [39, 40]. The resulting structures were deposited in the Protein Data Bank under the accession codes 2I61 and 2I62. Structure figures were generated with the program MOLMOL [41].

Results and discussion

Initial quantification of metal ion binding

Reconstituted forms of γ-E_c-1 with Zn^{II} and Cd^{II} were analysed for their metal ion content using flame-AAS and the 2-PDS assay and yielded M^{II} to thiol group ratios of 1:3 indicating the binding of two divalent metal ions per protein. The proposed metal stoichiometry was confirmed with mass spectrometry. For this two equivalents of Zn^{II} or four equivalents of Cd^{II}

ions were added to a solution of $Zn_2\gamma$-E_c-1, and the resulting mixture was analyzed with ESI-MS either at acidic or neutral pH. The spectrum at acidic pH shows the apoγ-E_c-1 species as expected, while at neutral pH exclusively $Zn_2\gamma$-E_c-1 or $Cd_2\gamma$-E_c-1 are observed despite the addition of an excess of the respective metal ion (Figure 2).

>> insert Figure 2 here (single column) <<

To corroborate this result, apoγ-E_c-1 was titrated with increments of Cd^{II} and UV-spectra were recorded (Figure 3). They show the formation of the typical ligand-to-metal charge transfer (LMCT) bands at 245-250 nm indicative for Cd^{II} coordination to thiolate groups.

>> insert Figure 3 here (single column) <<

These bands increase in absorptivity up to the addition of two equivalents Cd^{II} and remain constant thereafter. It was already shown that the full-length E_c-1 protein is able to coordinate six divalent metal ions and that four of them can be accommodated in the C-terminal β_E-domain [3, 10]. That the remaining two metal ions are bound within the N-terminal γ-domain was evidenced with ESI-MS measurements on a proteolytically digested Zn_6E_c-1 sample revealing the presence of a $Zn_2\gamma$-E_c-1 species [19]. In the same publication, a [^{113}Cd,^{113}Cd]-COSY spectrum of $^{113}Cd_6$Ec-1 shows cross peaks between two ^{113}Cd signals that originate from metal ions coordinated within the γ-domain and let to the proposal of a Cd_2Cys_6 cluster. The results with the separate γ-E_c-1 peptide presented here clearly demonstrate that the binding ability for two divalent metal ions is not restricted to the domain within the full-length protein. This validates our experimental approach to use the separate γ-E_c-1 sequence for the in-depth spectroscopic characterisation of the γ-domain of wheat E_c-1.

pH titrations of $Zn_2\gamma$-E_c-1 and $Cd_2\gamma$-E_c-1

pH titrations followed by UV spectroscopy were performed to investigate the pH dependent metal ion release. Though not tantamount, the obtained apparent pK_a values of the Cys

residues in presence of the respective metal ion are a good indication for the relative binding affinity of the metal ion to the MT. A number of apparent pK_a values for different Zn^{II} and Cd^{II} MTs were recently reviewed [13]. In the context of the study presented here, the pH stability of γ-E_c-1 in comparison to the full-length protein and the β_E-domain is of special interest. The UV spectra of the pH titration of Zn_2- and Cd_2γ-E_c-1 are depicted in Figure 4 as well as the plots of molar absorptivity at 230 nm (Zn^{II}-form) and 250 nm (Cd^{II}-form) against the respective pH values.

>> insert Figure 4 here (single column) <<

Fitting of the data was performed as described [21, 6] and the results are presented in more detail in the Supplementary Material. As the pK_a values obtained for both Zn_2γ-E_c-1 and Cd_2γ-E_c-1 were significantly higher than determined for the respective β_E- and full-length forms (Figure 5), also a titration of an equimolar mixture of both domains was performed. The resulting pK_a values for the mixed domains are settled in-between the values obtained for the respective γ- and β_E-domains, but are still significantly higher than the values for the full-length E_c-1 forms (Figure 5).

>> insert Figure 5 here (single column) <<

Hence it appears that not the mere presence but rather the close proximity of the respective other domain leads to the observed increased pH stability of the full-length protein. While basically possible it seems unlikely that the nature of the five amino acids SGAAA between the γ- and the β_E-domain, which were removed in the separately expressed domains, has a major influence as the residues are neither charged nor especially bulky or hydrophobic. So far, also no indications for any sort of interactions between the two domains were observed judging from the lack of corresponding NOE signals in the NMR experiments. Furthermore, ^{15}N dynamics data, in particular values of the $^{15}N\{^1H\}$-NOE, indicate that the linker comprising residues 26 to 30 is fully flexible [10]. One possible explanation for the low pK_a values of the full-length protein could be that the spatial proximity of the respective other

domain leads to a reduced solvent accessibility and hence to a deferred metal ion displacement by protons. Alternatively, formation of intermediate species in the full-length protein at decreasing pH values could occur slowing down the metal ion release process, i.e. migration of metal ions between the two domains or even transient generation of a new cluster arrangement. However, such species would not be detected in the structural investigation presented here, as the NMR experiments were performed at pH 6.9, while metal ion release only starts below 6.5 for the Zn^{II}- and 5.5 for the Cd^{II}-forms. Interesting to note is that the stabilizing effect of the respective other domain is obviously much more pronounced for the γ-domain, while the β_E-domain shows within the error limits the same apparent pK_a values as the full-length protein. Shifts in pK_a values present subtle probes into thermodynamic protein stability, and our data indicate that the γ-domain is intrinsically less stable than the β_E-domain when in isolation, although both are structured and capable of metal binding.

An additional surprising result was obtained, when evaluating the pH titration data for Zn_2γ-E_c-1 and Cd_2γ-E_c-1 more closely. The absorptivity values obtained from the curve fit with the equation considering two apparent pK_a values reveal a decrease by approximately one third for the first protonation step, characterized by pK_{a2}, i.e. $\Delta\varepsilon$ 2900 ± 400 M^{-1} cm^{-1} for Zn_2γ-E_c-1 and $\Delta\varepsilon$ 7200 ± 1700 M^{-1} cm^{-1} for Cd_2γ-E_c-1, and a decrease by two thirds for the second step, characterized by pK_{a1}, i.e. $\Delta\varepsilon$ 5700 ± 400 M^{-1} cm^{-1} for Zn_2γ-E_c-1 and $\Delta\varepsilon$ 17300 ± 1700 M^{-1} cm^{-1} for Cd_2γ-E_c-1 (see Supplementary Material). Disregarding the contribution of bridging thiolate ligands to the LMCT bands, which is considerably lower than the contribution of terminal thiolate ligands, the absorptivity decreases suggest the loss of two terminal metal-thiolate bonds in the first step and of four metal-thiolate bonds in the second. This suggests that in the first step one metal ion is released and hence the contribution of two terminal and two bridging metal-thiolate bonds is lost, while in the second step the second metal ion is

released and hence the contribution of the residual four metal-thiolate bonds disappears. As a result, the two metal ions in γ-E_c-1 seem to be released at pH values approximately 0.6-0.7 units apart and this might also be an indication that γ-E_c-1 contains two metal ion binding sites with different affinities.

Extended X-ray absorption fine structure (EXAFS) spectroscopy of Zn_2γ-E_c-1

EXAFS spectra were recorded to analyse the coordination environment of the Zn^{II} ions in Zn_2γ-E_c-1. The results reveal the presence of four sulfur ligands and no contribution of lighter ligands with N- or O-donor atoms within the error limits. Zn-S distances are with 2.332(3) Å in the normal range for Zn^{II} coordination by thiol ligands (Figure 6, Table 1).

>> insert Figure 6 (single column) and Table 1 here <<

Assuming the presence of a Zn-Zn interaction with a distance of 3.163(6) Å improves the Fit Index significantly from 0.2988 to 0.2141. However, the error range for the corresponding average number of ligands is relatively high. These findings together with the results from concentration and ESI-MS measurements presented above strongly suggests the formation of a Zn_2Cys_6 metal-thiolate cluster with four terminal and two bridging thiolate groups. Such a cluster is in accordance with the Cd_2Cys_6 cluster proposed to be formed in $^{113}Cd_6$Ec-1 based on the [^{113}Cd,^{113}Cd]-COSY spectrum mentioned above [19].

NMR solution structures of the separate Zn_2γ-E_c-1 and Cd_2γ-E_c-1 peptides

Except for the first two amino acids Gly and Ser, which were engineered to improve proteolytic cleavage of the GST-fusion protein by thrombin all residues could be identified with 3D ^{15}N-resolved NOESY and TOCSY NMR experiments in case of the Cd^{II} form or with 3D ^{15}N-resolved NOESY, 2D TOCSY and [^{15}N, ^{1}H]-HSQC experiments for the Zn^{II}

form. Experiments with the NMR active ^{113}Cd nucleus were performed to probe the metal ion coordination sphere. [^{113}Cd, ^{1}H]-HSQC spectra allow observing cross peaks based on ^{3}J couplings between the H_β protons of the Cys residues and the respective coordinated Cd^{II} ions. In theory, each of the 12 H_β protons of the six Cys residues present in the peptide should display a ^{3}J coupling to one $^{113}Cd^{II}$ ion, or in the case of bridging thiolate ligands, to two Cd^{II} ions. As shown in Figure 7 indeed the majority of Cys residues correlate to metal ions, however, not two as expected but rather three possible bridging Cys residues were identified.

>> insert Figure 7 here (single column)<<

Despite differences in size and electronegativity Cd^{II}- and Zn^{II}-forms of MTs have been interchangeably used for structural studies [32,101,102]. In case of the γ-E_c-1 domain such an assumption is justified by the reasonable agreement of proton chemical shifts in the two forms (Figure 8).

>> insert Figure 8 here (single column) <<

Chemical shift assignment was based on the sequence-specific sequential resonance assignment procedure developed by Wüthrich and coworkers [32]. Overall, completeness of proton assignment was 99%. No long-range NOEs reflecting contacts of residues from the C- and N-terminal region were observed in the NOESY spectra. Pro-12 (in contrast to Pro-14) was shown to be connected via a cis peptide bond to the previous residue in both metal isoforms (Supplementary Fig. 1), as deduced from comparably strong NOEs of the sequential alpha protons. The comparison of backbone amide ^{1}H and ^{15}N chemical shifts for residues of the γ-domain indicates that differences as large as 0.4 or 1.1 ppm are observed between the Zn- and Cd-species, respectively (Supplementary Fig. 2). The largest differences are not limited to residues that are involved in metal coordination, but also include some of the residues in the small loop regions. A comparison of the amide proton and nitrogen chemical shifts of Zn_2γ-E_c-1 with the values previously determined on the full-length Zn_6E_c-1 protein reveals that chemical shift differences are negligible and limited to the terminal residues

(Supplementary Fig. 2). The latter are expected to be different due to the slightly N-terminally modified sequence (GlySer instead of Met) or due to the additional presence of the C-terminal β_E-domain in the full-length species. As mentioned above, a somewhat surprising result of the analysis is that while the analysis of the pK_a values indicated differences between corresponding segments in the isolated γ-domain compared to the full-length protein no such differences could be detected in the backbone amide chemical shifts. We speculate that there may be contacts between the two domains that, however, are very transient (and possibly also unspecific) in nature.

Initial structures calculated without addition of explicit metal-Cys(Sγ) restraints (Supplementary Fig. 3) converge for the amino acid residues Gly-2 to Gly-18. However the positions of the C-terminal residues and of the thiol groups of the Cys residues deviate substantially. When upper distance restraints were added that enforced tetrahedral geometry and metal sulphur distances derived from EXAFS experiments also the calculations for the C-terminal part of the structure converged. While Cys-9 (numbering according to amino acid sequence given in Fig. 1) could be unambiguously identified as a bridging Cys residue based on the [^{113}Cd,^{1}H]-HSQC experiment, the nature of the second bridging Cys residue could not be experimentally established. Accordingly, independent structure calculations were started assuming the bridging residues to be i) Cys-9 and 21, ii) Cys-9 and 3 and iii) Cys-9 and 13 with all other Cys residues coordinating in terminal fashion. The calculation using Cys-9/13 as bridging residues resulted in no low-energy conformer and was therefore excluded from further analysis. The resulting structures containing the metal cluster arrangements Cys-9/21 and Cys-9/3 are representatively shown for Zn_2γ-E_c-1 in Figure 9, and the statistics from the corresponding structure calculations are summarized in Table 2.

>> insert Figure 9 (single column) and Table 2 here <<

Similar to previously determined structures of metallothioneins the γ-domain of E_c-1 is devoid of regular secondary structure. Superposition of backbone atoms result in RMSD values of

0.62 to 0.8 Å for backbone atoms of residues 2 to 22, and 1.3 to 1.5 for all heavy atoms, and the values are very similar for the Cd^{II}- or Zn^{II}-loaded isoforms (see Table 2). The overall fold resembles a hook, in which the stem part is formed by the segments comprising Cys7-9 and Cys19-21, and the loop by the coordination of Cys-13 to the metal. Two loops bridge the latter residue to the next metal-anchoring residues Cys-9 and Cys-19. Coordination of Cys-3 brings the N terminal segment into proximity. No significant differences in conformation that were unambiguously supported by the NOEs were observed between the Cd^{II}- and Zn^{II}-loaded peptides despite the fact that in part substantial chemical shift differences are observed (*vide supra*). A superposition of the backbone atoms of conformers, in which either Cys-3 or Cys-21 were constrained to be the bridging ligands, revealed that only small structural adaptations were necessary to transform one form into the other. Considering that only upper-distance limits were derived from the NOEs and taking the inherent dynamics of the system as well as the low proton density in metallothioneins, that are largely devoid of regular secondary structure or tertiary contacts, into account we feel that no sound statements on structural differences of the Zn^{II}- or Cd^{II}-loaded species can be made on the basis of the present data. Moreover, the lack of explicit ^{113}Cd-Cys(Hβ) cross peaks in the [^{113}Cd,^{1}H]-HSQC experiment for these residues, and the fact that the target functions of the calculated conformers are very similar precludes unambiguous determination of the nature of the second bridging Cys residue. Whether this is due to the fact that the coordination mode in the peptide changes dynamically or whether the NMR data simply are insufficient to describe a unique coordination mode remains unclear presently.

A $M^{II}_2Cys_6$ cluster as identified in the γ-domain is unprecedented for MTs so far, but a very similar Zn_2Cys_6 cluster was previously observed in the transcription factor GAL4 from *Saccheromyces cerevisiae* [42]. Also here the metal-Cys connectivities were probed by replacement of Zn^{II} ions by $^{113}Cd^{II}$. Since the two ^{113}Cd resonances at 669 and 707 ppm are well separated it was possible to identify the bridging Cys residues using selectively

decoupled [^{113}Cd,^{1}H]-HSQC spectra. However, such an experiment is not feasible in the case of $Cd_2\gamma$-E_c-1 owing to the very small chemical shift difference of only 2 ppm. Nevertheless, two further peculiarities in the NMR spectra corroborate the concomitant presence of two different, probably interchanging cluster arrangements. Firstly, in $^{113}Cd_2\gamma E_c$-1 TOCSY spectra cross peaks due to the geminal $H\beta_2$- $H\beta_3$ correlation for the putative bridging Cys residues 3 and 21 are significantly broadened, and the corresponding correlation for Cys 9 is broadened beyond detection, indicating the presence of exchange processes. Secondly, in contrast to spectra recorded on the full-length protein [19], no mutual coupling was observed in the [^{113}Cd,^{113}Cd]-COSY spectrum of $^{113}Cd_2\gamma$-E_c-1, which might again be explained by intermediate exchange processes occurring in the isolated domain.

NMR solution structure of $Zn_2\gamma$-E_c-1 as part of the full-length Zn_6E_c-1 protein and comparison to the separate $Zn_2\gamma$-E_c-1 peptide

Spectroscopic and spectrometric studies [3, 10, 19, 43] have revealed that wheat Zn_6E_c-1 is a two-domain protein. The larger C-terminal domain, termed extended-β or β_E, consists of 51 amino acids and embeds a mononuclear $ZnCys_2His_2$ site as well as a trinuclear Zn_3Cys_9 metal-thiolate cluster with similarity to the β-domain of the vertebrate MTs. As described above the smaller 24 amino acids long N-terminal domain, γ-E_c-1, folds around a Zn_2Cys_6 cluster. Chemical shift mapping accompanied by ^{15}N relaxation experiments was used to confirm identical folds of both the β_E-domain in form of the separately expressed peptide as well as being part of the full-length Zn_6E_c-1 protein. To confirm that this is also true for the γ-domain, chemical shift assignment and identification of close contacts from NOESY spectra was performed for both the isolated peptides (Cd^{II}- and Zn^{II}-isoforms) of the γ-domain and for the corresponding part in the full-length protein. Similar chemical shifts and NOESY

crosspeaks (Figure 8) indicate analogous peptide folding. A comparison of the solution structure bundle calculated for the embedded and for the independent γ-domain (Zn^{II}-isoform, Cys-9/21 bridging) is displayed in the Supplementary Material. Indeed, only minor differences between the two conformations are observed.

Comparison of $Zn_2\gamma$-E_c-1 with the Zn_2Cys_6 cluster in GAL4

As mentioned above, Zn_2Cys_6 clusters were so far only structurally described in yeast transcription factors [42, 44, 45]. Amino acid sequence alignments of the latter reveal a completely conserved Cys distribution pattern and a high conservation of Lys residues, which play a major role for the interaction of these proteins with DNA (Figure 10). In contrast, the Cys distribution pattern of the γ-E_c-1 domain differs significantly from that of the transcription factors, and only three positively charged residues, one Lys and two Arg, are present. In addition, while the fold of the protein backbone in the yeast transcription factors can be described as a loop, the backbone of γ-E_c-1 is S-shaped or resembles a hook (Figures 9 and 10). Taken together, despite the similarity of the metal-thiolate clusters, recognition of DNA by γ-E_c-1 in the same fashion as observed for the yeast transcription factors seems unlikely.

>> insert Figure 10 here (double column) <<

Conclusions

Complementing our investigation of the $Zn_4\beta_E$-E_c-1 domain including the determination of its solution structure by NMR [10, 19] we complete now the second part of the puzzle by presenting a study of the properties and the solution structure of the γ-domain of wheat E_c-1.

ESI-MS experiments in conjunction with F-AAS measurements and metal ion titrations followed with UV spectroscopy clearly confirm the ability of the N-terminal E_c-1 fragment to coordinate two Zn^{II} or Cd^{II} ions even in the absence of the β_E-domain. Tetrahedral tetrathiolate coordination of the bound Zn^{II} ions is established by EXAFS measurements in addition to the presence of a short Zn-Zn distance of 3.16 Å. pH titrations of $Zn_2\gamma$-E_c-1 and $Cd_2\gamma$-E_c-1 reveal higher apparent pK_a values of the Cys residues than previously determined for the β_E-domain and full-length E_c-1. This earlier protonation of thiolate ligands is paralleled by an increased peptide backbone flexibility compared to the β_E-domain [10]. A pH titration of an equimolar mixture of the γ- and the β_E-domain yields intermediate pK_a values, which however differ from the values obtained with the full-length protein. This might indicate a yet unidentified interaction between the two domains in the full-length protein that increases the pH stability especially of the $M^{II}{}_2Cys_6$ cluster of the γ-domain. Owing to the low percentage or even lack of regular secondary structure in MTs the metal clusters critically contribute to the overall protein fold. Hence only when the metal-coordinating residues have been identified the structure can be determined correctly. In case of the γ-domain [^{113}Cd,^{1}H]-HSQC spectra indicated three possible metal ion-to-Cys connectivities, one of which could be eliminated during the structure calculation. Based on the ^{113}Cd NMR and ^{1}H NMR studies of the separate $Zn_2\gamma$-E_c-1 and $Cd_2\gamma$-E_c-1 peptides as well as of the embedded domain in the full-length protein we propose the presence of a highly dynamic metal cluster, possibly switching between two slightly different cluster arrangements recruiting either Cys-3 or Cys-21 as the second bridging thiolate ligand. This flexibility is in line with the observed decreased rigidity of the γ-domain compared to the β_E-domain as observed in ^{15}N relaxation experiments [10]. Overall, the structures of the separate $Zn_2\gamma$-E_c-1 and $Cd_2\gamma$-E_c-1 peptides show only minor differences within the error limits In addition, when monitoring the chemical shifts of the backbone amide protons and nitrogen atoms in the 24-residue N-terminal segment of Zn_6E_c-1

and in the separate $Zn_2\gamma$-E_c-1 peptide only small differences are observed. Hence the solution structure of the separately expressed γ-E_c-1 peptide can be reliably taken as a model for the γ-domain in the full-length E_c-1 protein.

Acknowledgements

We thank Prof. Peter Güntert for refining the CYANA structures with a full force field. This work was supported by the Swiss National Science Foundation (SNF Förderungsprofessur PP002-119106/1 to E.F.).

Literature

1. Vallee BL (1979) In: Kägi JHR, Nordberg M (eds) Metallothionein. Birkhäuser Verlag, Basel, pp. 19-40.
2. Binz P-A, Kägi JHR (1999) In: Klaassen C (ed) Metallothionein IV. Birkhäuser Verlag, Basel, pp. 7-13.
3. Peroza EA, Freisinger E (2007) J. Biol. Inorg. Chem. 12:377-391.
4. Hanley-Bowdoin L, Lane BG (1983) Eur. J. Biochem. 135:9-15.
5. Lane BG, Kajioka R, Kennedy TD (1987) Biochem Cell Biol 65:1001-1005.
6. Blindauer CA, Harrison MD, Parkinson JA, Robinson AK, Cavet JS, Robinson NJ, Sadler PJ (2001) Proc. Natl. Acad. Sci. U S A 98:9593-9598.
7. Braun W, Vašák M, Robbins AH, Stout CD, Wagner G, Kägi JHR, Wüthrich K (1992) Proc. Natl. Acad. Sci. U S A 89:10124-10128.
8. Narula SS, Brouwer M, Hua Y, Armitage IM (1995) Biochemistry-Us 34:620-631.
9. Riek R, Prêcheur B, Wang Y, Mackay EA, Wider G, Güntert P, Liu A, Kägi JHR, Wüthrich K (1999) J. Mol. Biol. 291:417-428.

10. Peroza EA, Schmucki R, Güntert P, Freisinger E, Zerbe O (2009) J. Mol. Biol. 387:207-218.
11. Palmiter RD (1998) Proc. Natl. Acad. Sci. U S A 95:8428-8430.
12. Coyle P, Philcox JC, Carey LC, Rofe AM (2002) Cell. Mol. Life Sci. 59:627-647.
13. Freisinger E (2008) Dalton Trans.:6663-6675.
14. Kawashima I, Kennedy TD, Chino M, Lane BG (1992) Eur. J. Biochem. 209:971-976.
15. Finkelstein RR, Gampala SSL, Rock CD (2002) Plant Cell 14:S15-S45.
16. Laudencia-Chingcuanco DL, Stamova BS, You FM, Lazo GR, Beckles DM, Anderson OD (2007) Plant Mol. Biol. 63:651-668.
17. Pedersen AO, Jacobsen J (1980) Eur. J. Biochem. 106:291-295.
18. Freisinger E (2007) Inorg. Chim. Acta 360:369-380.
19. Peroza EA, Al Kaabi A, Meyer-Klaucke W, Wellenreuther G, Freisinger E (2009) J. Inorg. Biochem. 103:342-353.
20. Korbas M, Marsa DF, Meyer-Klaucke W (2006) Rev. Sci. Instrum. 77:1-5.
21. Wellenreuther G, Parthasarathy V, Meyer-Klaucke W (2010) J. Synchrotron Radiat. 17:25-35.
22. Binsted N, Strange RW, Hasnain SS (1992) Biochemistry-Us 31:12117-12125.
23. Braunschweiler L, Ernst RR (1983) J. Magn. Reson. 53:521-528.
24. Bax A, Davis DG (1985) J. Magn. Reson. 65:355-360.
25. Kumar A, Ernst RR, Wüthrich K (1980) Biochem. Biophys. Res. Commun. 95:1-6.
26. Macura S, Ernst RR (1980) Mol. Phys. 41:95-117.
27. Otting G (1990) J. Magn. Reson. 86:496-508.
28. Rance M, Bodenhausen G, Wagner G, Wüthrich K, Ernst RR (1985) J. Magn. Reson. 62:497-510.
29. Palmer AG, Cavanagh J, Wright PE, Rance M (1991) J. Magn. Reson. 93:151-170.
30. Kay LE, Keifer P, Saarinen T (1992) J. Am. Chem. Soc. 114:10663-10665.

31. Vašák M (1998) Biodegradation 9:501-512.
32. Wüthrich K (1986) NMR of proteins and nucleic acids. Wiley-Interscience, New York.
33. Bartels C, Xia TH, Billeter M, Güntert P, Wüthrich K (1995) J. Biomol. NMR 6:1-10.
34. Keller RLJ (2004) Computer aided resonance assignment tutorial. CANTINA Verlag, Goldau.
35. Güntert P, Mumenthaler C, Wüthrich K (1997) J. Mol. Biol. 273:283-298.
36. Herrmann T, Güntert P, Wüthrich K (2002) J. Mol. Biol. 319:209-227.
37. Güntert P (2003) Progr. Nucl. Magn. Reson. Spectrosc. 43:105-125.
38. Cornell WD, Cieplak P, Bayly CI, Gould IR, Merz KM, Ferguson DM, Spellmeyer DC, Fox T, Caldwell JW, Kollman PA (1995) J. Am. Chem. Soc. 117:5179-5197.
39. Koradi R, Billeter M, Güntert P (2000) Comput. Phys. Commun. 124:139-147.
40. Luginbühl P, Güntert P, Billeter M, Wüthrich K (1996) J. Biomol. NMR 8:136-146.
41. Koradi R, Billeter M, Wüthrich K (1996) J. Mol. Graphics 14:51-55.
42. Baleja JD, Thanabal V, Wagner G (1997) J. Biomol. NMR 10:397-401.
43. Leszczyszyn OI, Schmid R, Blindauer CA (2007) Proteins: Structure, Function, and Bioinformatics 68:922-935.
44. Gardner KH, Anderson SF, Coleman JE (1995) Nat. Struct. Mol. Biol. 2:898-905.
45. Marmorstein R, Harrison S (1994) Genes Dev. 8:2504-2512.

Table 1 EXAFS refinement parameters for $Zn_2\gamma$-E_c-1

N	*M ··· L*	*R (Å)*	*$2\sigma^2$ (Å^2)*	*EF (eV)*	*Φ*
$Zn_2\gamma$-E_c-1		ΔE= 13 eV – 770 eV		$E_{0,Zn}$= 9662 eV	
4	Zn ··· S	2.332(3)	0.0134(5)	-7.6(5)	0.2141
0.5(3)	Zn ··· Zn	3.163(6)	0.006(3)		

Best models with average numbers (N) of ligand atoms (L), their distance to the metal ion (R), the respective Debye-Waller factor ($2\sigma^2$), the Fermi energy for all shells (EF), and the Fit Index (Φ), indicating the quality of the fit are shown. The total error is estimated to 0.01 Å or smaller for first shell distance and 0.05 to 0.1 Å for the metal-metal contribution. In parentheses the numerical error margins are given on the 2σ level.

1 **Table 2 Statistics of structure calculations:**

2

	Cd3*	Cd21*	Zn3*	Zn21*	Zn3(full)*	Zn21(full)*
NMR distance restraints						
Total NOE	374	372	462	463	307	310
Short range: |i−j|≤1	322	321	396	395	268	268
Medium range: 1>|i−j|>5	61	58	69	70	47	44
Long range: |i−j|≥5	15	13	20	20	13	15
Maximal distance restraint violation (Å)	0.11	0.11	0.11	0.19	0.16	0.44
AMBER energies (kcal/mol)						
Total (mean±SD)	−679 ± 76	−711 ± 43	−697 ± 70	−693 ± 75	−679 ± 52	−641 ± 67
van der Waals	−14 ± 4	−7 ± 5	−12 ± 5	−12 ± 6	−9 ± 5	−8 ± 7

RMSDs from idealized geometry						
Bond lengths (Å)	0.0142 ± 0.0002	0.0138 ± 0.0002	0.0136 ± 0.0002	0.0142 ± 0.0002	0.0138 ± 0.0002	0.0138 ± 0.0002
Bond angles (°)	2.15 ± 0.06	2.03 ± 0.06	1.94 ± 0.06	2.42 ± 0.06	2.11 ± 0.06	2.11 ± 0.06
Ramachandran plot statistics (%)						
Residues in most favored regions	80.9	70.9	74.4	69.4	65.6	63.5
Residues in additionally allowed regions	18.2	28.5	24.7	28.5	32.4	32.4
Residues in generously allowed regions	0.9	0.6	0.9	1.8	2.1	3.2
Residues in disallowed regions	0	0	0	0.3	0	0.9
RMSDs from the mean coordinates (Å)						

N, Cα, and C′ of residues 2-22	0.70±0.14	0.69 ± 0.33	1.06 ± 0.34	0.97 ± 0.25	1.29 ± 0.44	1.50 ± 0.45
Heavy atoms of residues 2-22	1.37±0.26	1.45 ± 0.37	1.76 ± 0.35	1.54 ± 0.27	1.97 ± 0.43	2.26 ± 0.46

1

2 * The number describes the residue that presents the second bridging Cys moiety (in addition to Cys-9; see text). Numbering is performed with

3 respect to the sequence of the full-length protein as given in Fig. 1.

4

Figure legends

Fig. 1 Amino acid sequence of full-length wheat E_c-1 with the cysteine-rich metal ion coordinating regions highlighted in grey (top) as well as a schematic representation giving the sort and number of coordinating amino acids. The N-terminal Cys-rich region harbors the herein described Zn_2Cys_6 cluster, while the central and C-terminal regions together form the $Zn_4\beta_E$-domain.

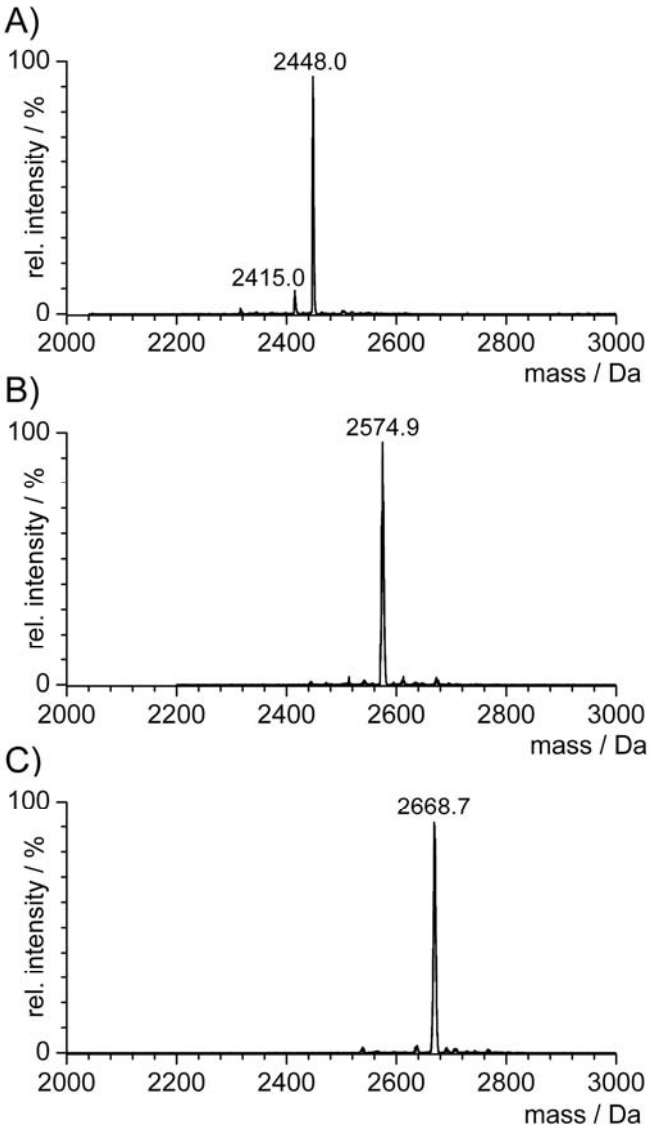

Fig. 2 Deconvoluted ESI-MS spectra of (A) γ-E_c-1 in form of the metal-depleted apo-form at pH 2 (calc. mass 2448.0 Da), (B) Zn_2γ-E_c-1 (calc. 2574.7 Da) or (C) Cd_2γ-E_c-1 (calc. 2668.8 Da), both at pH 7.5.

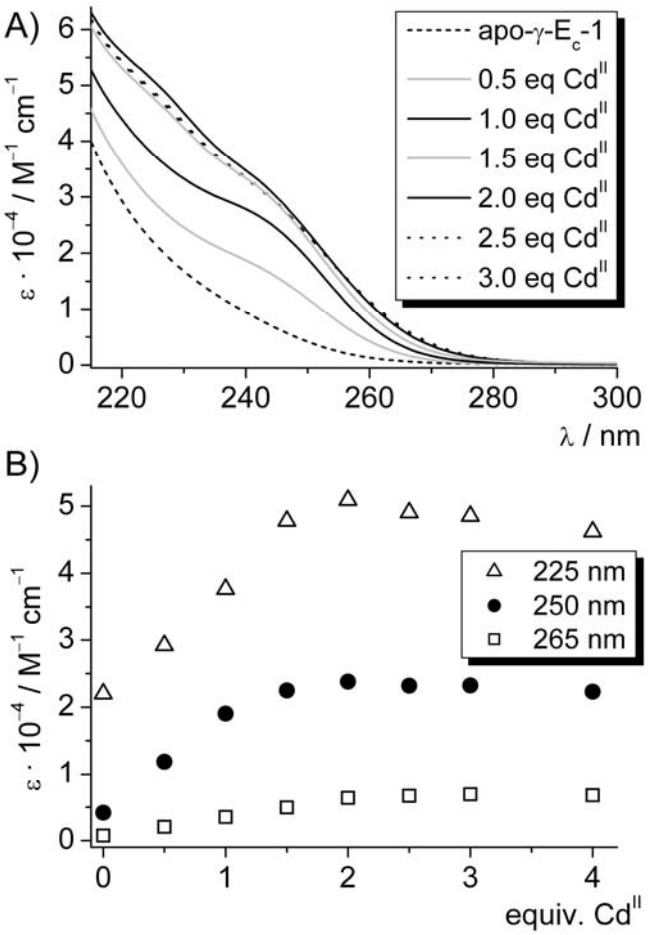

Fig. 3 (A) UV spectra of the stepwise reconstitution of apoγ-E_c-1 with Cd^{II} ions showing the evolution of the S→Cd^{II} LMCT bands around 250 nm. (B) Plots of molar absorptivity at 225, 250, and 265 nm against the number of equiv. of Cd^{II} ions added all reaching the maximum value after addition of two equiv.

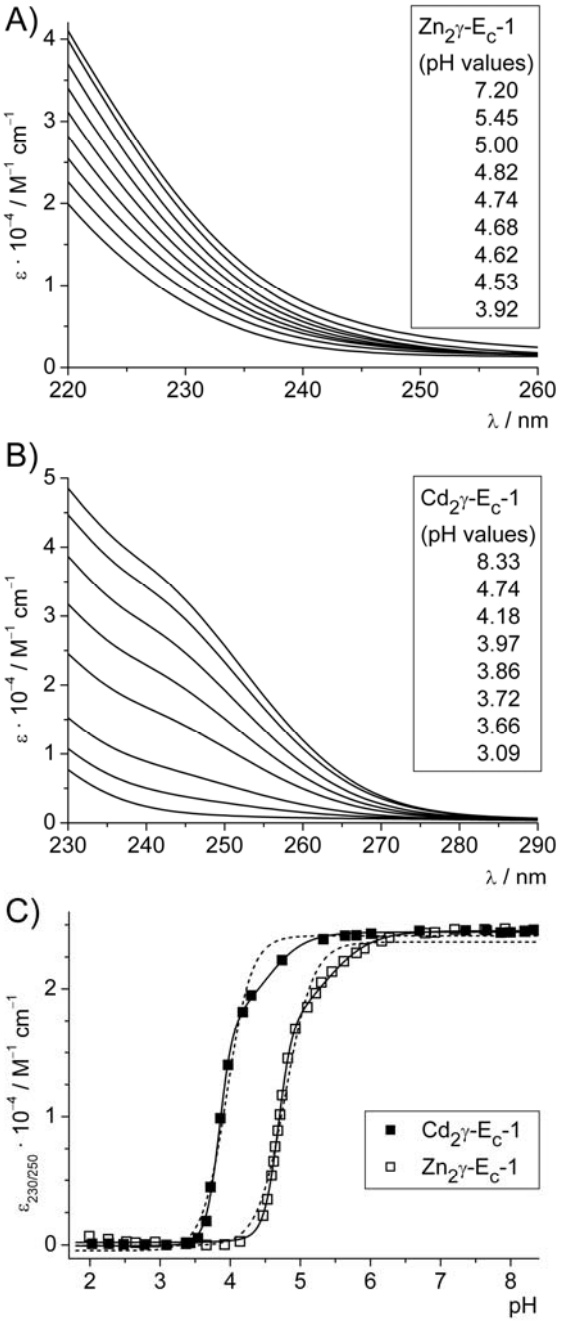

Fig. 4 Representative UV spectra of the titration of (A) Zn_2- and (B) $Cd_2\gamma$-E_c-1 with increasing amounts of HCl. (C) Plots of molar absorptivity at 230 nm for the Zn^{II}- and at 250 nm for the Cd^{II}-form versus pH. To allow better comparability, the values obtained for the apo-forms in both titrations were shifted to zero and in addition the plot of the Zn^{II}-form was normalized to the values obtained for the Cd^{II}-form. Curve fits were performed with equations considering one (dashed lines) or two apparent pK_a values (solid lines) as described in the Suppl. Mat.

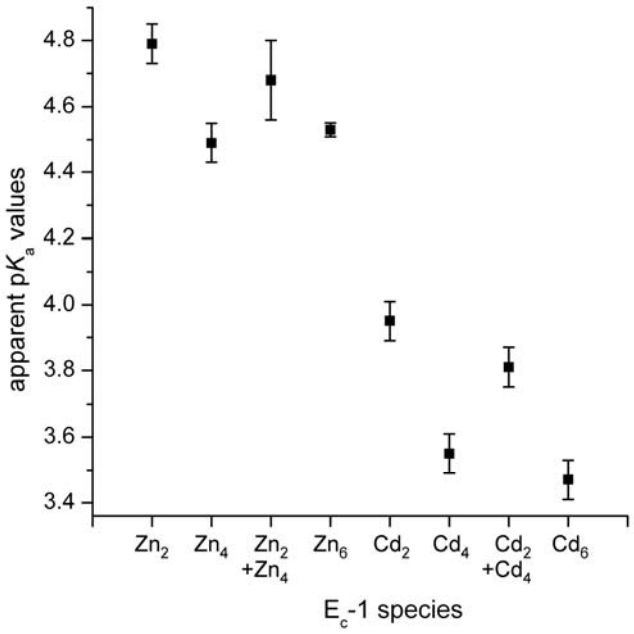

Fig 5 Apparent pK_a values of the Cys residues in γ-, β_E- and full-length wheat E_c-1 in presence of Zn^{II} or Cd^{II} ions. The error bars show the 3σ error range. From left to right: 4.79(6), 4.49(6), 4.68(12), 4.530(21), 3.95(6), 3.55(6), 3.81(6), and 3.47(6).

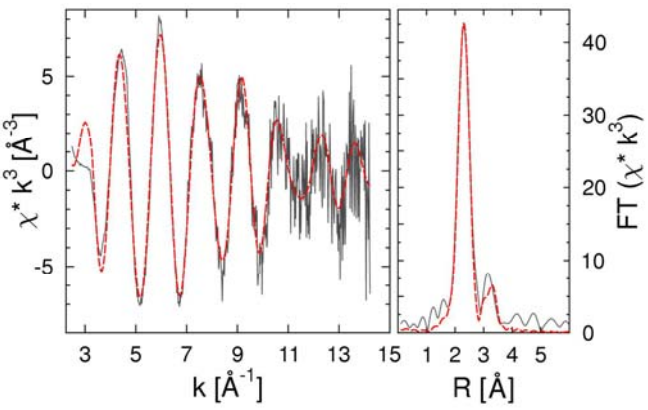

Fig. 6 EXAFS (left) and corresponding Fourier transform (right) of Zn_2γ-E_c-1. The EXAFS is dominated by a single frequency, originating from sulfur backscattering. In the refinement no other first shell contribution could be identified. In line with this result the Fourier transform is dominated by a single peak at 2.3 Å. The additional peak above 3 Å is refined as metal-metal contribution, indicative of bridging sulfur ligands. The corresponding parameters are given in Table 1.

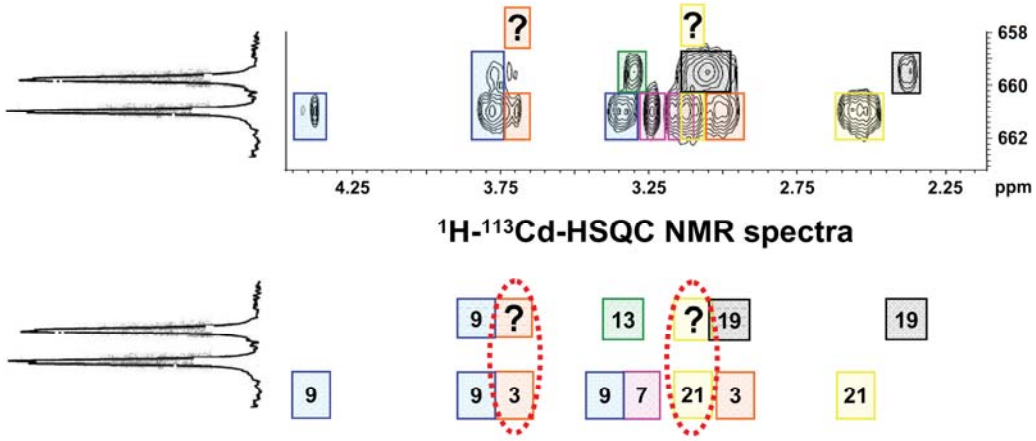

Fig. 7 The 1D ^{113}Cd NMR spectrum of $Cd_2\gamma$-E_c-1 shows two doublets representing the two Cd^{II} ions. The 2D ^{113}Cd-^{1}H-HSQC NMR spectrum allows two possible solutions for the bridging Cys residues: Cys-9/3 and Cys-9/21. The assignment of cross peaks to Cys residues is schematically depicted in the lower part.

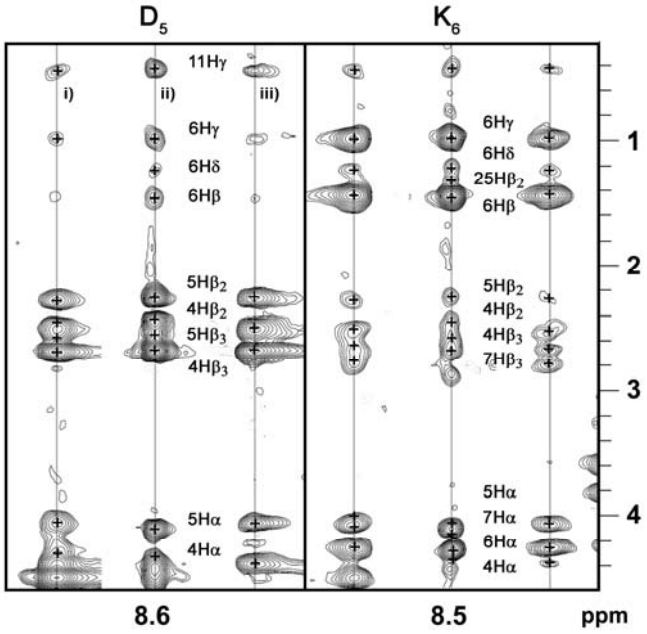

Fig. 8 Comparison of the 3D ^{15}N-^{1}H-^{1}H NOESY NMR slices of Asp-5 and Lys-6 depicted for the separate $Zn_2\gamma$-E_c-1 (i) and $Cd_2\gamma$-E_c-1 (ii) peptides as well as for the $Zn_2\gamma$-E_c-1 domain (iii) within the full-length protein. Assigned NOE cross peaks are labelled. The high degree of NOE pattern homology is apparent.

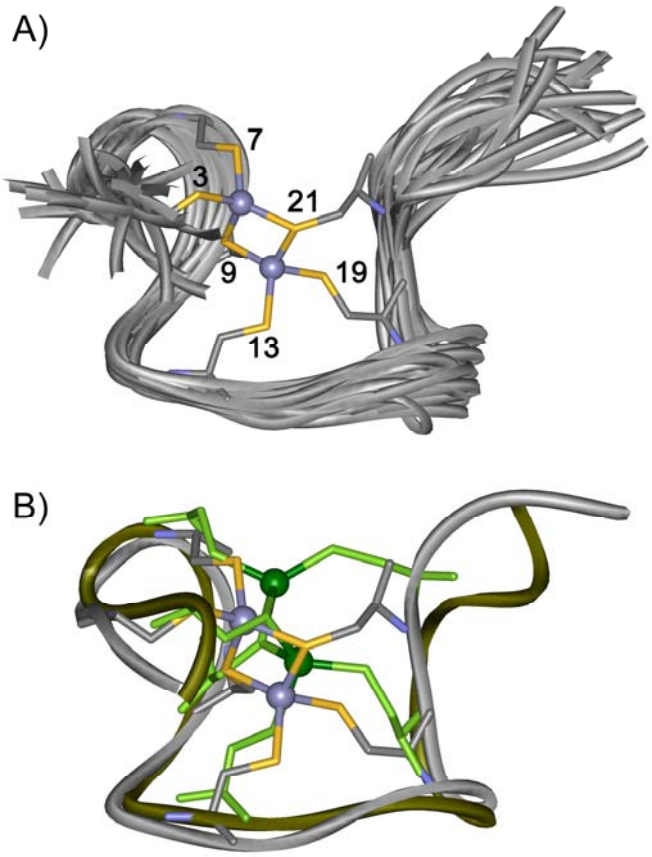

Fig. 9 (A) Structure bundle for $Zn_2\gamma$-E_c-1 showing the metal cluster arrangement Cys-9/21. The backbones are shown in gray, the Cys residues of one representative structure in stick mode and the two corresponding Zn^{II} ions as light blue spheres. Cys residues are numbered according to their position in the amino acid sequence given in Fig. 1. (B) Backbone overlay of two representative structures of $Zn_2\gamma$-E_c-1 with Cys-9/21 connectivity as in (A) and with Cys-9/3 arrangement (olive backbone, Cys residues as green sticks, Zn^{II} ions as dark green spheres).

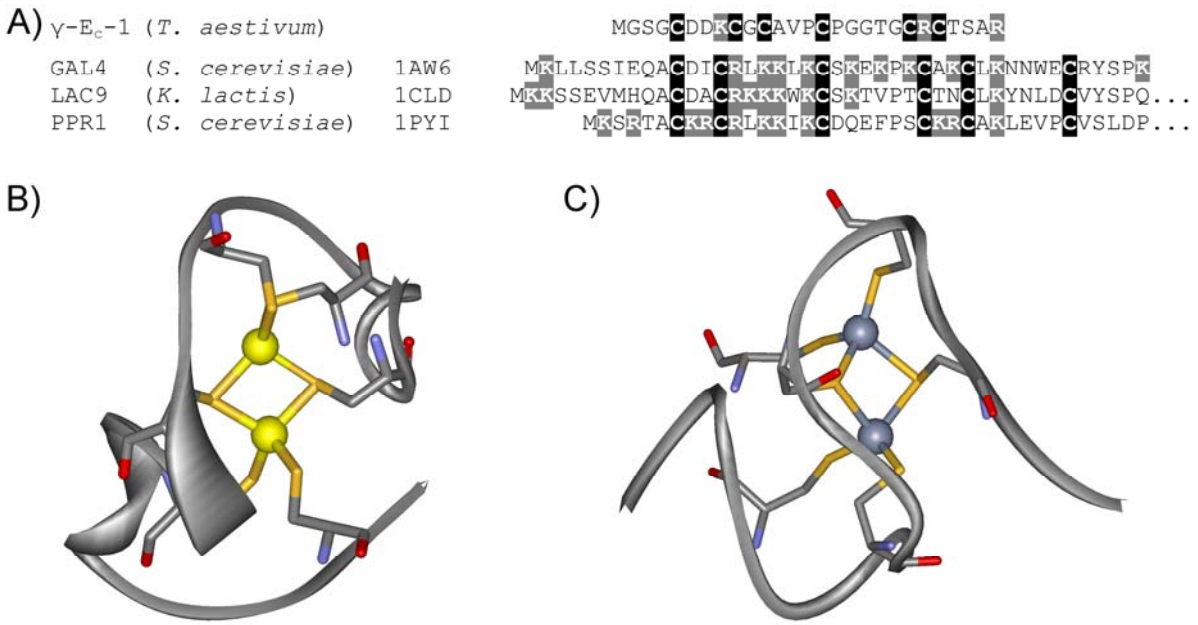

Fig. 10 (A) Amino acid sequence of γ-E_c-1 and alignment of the sequences from the three yeast transcription factors GAL4, LAC9, and PPR1 with the species name and PDB accession code given. Cys residues are highlighted with a black, Lys and Arg residues with a grey background. NMR solution structure of (B) Cd_2GAL4 [42] and (C) Zn_2γ-E_c-1 with the metal ions drawn as yellow or blue-grey spheres and the Cys residues presented in stick mode. The N-terminus is positioned to the (upper) right, respectively.